JOURNAL OF THE AMERICAN CHEMICAL SOCIETY
Article
pubs.acs.org/JACS

$CsPbCO_3F$: A Strong Second-Harmonic Generation Material Derived from Enhancement via p−π Interaction

Guohong Zou,[†,‡] Ling Huang,[‡] Ning Ye,*[,†] Chensheng Lin,[†] Wendan Cheng,[†] and Hui Huang[‡]

[†]Key Laboratory of Optoelectronic Materials Chemistry and Physics, Chinese Academy of Sciences, Fujian Institute of Research on the Structure of Matter, Fuzhou, Fujian 350002, P. R. China

[‡]New Materials R&D Center, Institute of Chemical Materials, China Academy of Engineering Physics, Chengdu, Sichuan 621900, P. R. China

S *Supporting Information*

ABSTRACT: The combination of Pb^{2+} cations with lone-pair electrons and F^- anions with the largest electronegativity into the carbonate generates a new nonlinear optical material, $CsPbCO_3F$, with the largest powder second-harmonic generation (SHG) response among carbonates of about 13.4 times that of KDP (KH_2PO_4), and transparency over the near-UV to middle-IR region. The optical characterization of the compound indicates that it is phase matchable. Its crystal structure exhibits the stacking of $[CsF]_\infty$ and $[Pb(CO_3)]_\infty$ layers, and the coplanar alignment of $[CO_3]$ triangles which are oriented in the same direction. Yet the Pb^{2+} cation has an inert or nonstereoactive lone-pair, as indicated by its more spherical shape. Theoretical calculations confirm that the extremely large SHG efficiency indeed originates from enhancement via p−π interaction between Pb^{2+} and $[CO_3]^{2-}$ within the $[Pb(CO_3)]$ layers.

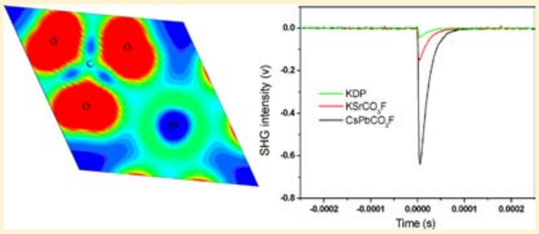

INTRODUCTION

The increasing importance of nonlinear optical (NLO) crystals,[1−5] especially those producing UV coherent light, has prompted the continuous search for new NLO crystals with high NLO coefficients and wide UV transparency. In the past decades, many efforts have been made to understand the relationship between the composition/structure and the NLO properties, which is critical in the development of new NLO crystals. The Anionic Group Theory proposed by Chen et al. states that the overall crystal nonlinearity is the geometrical superposition of the microscopic second-order susceptibility of the NLO-active anionic groups (structural units). This theory has been very successful in guiding the development of ultraviolet (UV) and deep UV NLO crystals in borates.[6,7] The macroscopic optical responses of the UV and deep-UV NLO borates are dominated by boron−oxygen anionic groups such as $[B_3O_6]^{3-}$ in β-BaB_2O_4 (BBO),[8,9] $[B_3O_7]^{5-}$ in LiB_3O_5 (LBO),[10,11] $[BO_3]^{3-}$ in $KBe_2BO_3F_2$ (KBBF),[12] and $Sr_2Be_2B_2O_7$ (SBBO),[13] and $[BO_4]^{5-}$ in SrB_4O_7.[14] In particular, the planar $[BO_3]^{3-}$ anionic group possesses a relatively large microscopic second-order susceptibility and moderate birefringence, so it is considered to be the best NLO basic structural unit for UV and deep-UV light generation.[15,16] Analogous to the $[BO_3]^{3-}$ group, the $[CO_3]^{2-}$ anionic group is expected to be a good NLO microstructural unit since it has the similar planar triangle structure with π-conjugated molecular orbital which can produce large second-order susceptibility. Thus, materials with $[CO_3]^{2-}$ groups have invoked specific interests, although reports on new carbonate NLO crystals are very scarce partly due to the difficulty of single crystal growth.[17] In our previous research, we have discovered a new series of alkaline and alkaline earth fluoride carbonates $MNCO_3F$ (M = K, Rb, Cs; N = Ca, Sr, Ba).[18] They are very promising as UV NLO materials for practical applications despite their moderate second harmonic generation (SHG) coefficients. On the basis of the relationship between the structure and overall NLO properties, two approaches for producing large NLO effects have been proposed. The first approach is to choose favorable structural units and have them parallel aligned. The second is to increase the density of the NLO structural units. In $KSrCO_3F$,[18] alkaline and alkaline earth fluoride carbonates, the $[CO_3]$ triangles are coplanarly aligned and oriented in the same direction with high density. To further enhance the SHG, other polarization groups have been introduced, such as distorted polyhedra with a d^0 cation center resulting from a second-order Jahn−Teller effect,[19−21] polar displacement of a d^{10} cation center,[22,23] or distortion from the stereochemically active lone pair effect of the cation,[24,25] or borate π-orbital systems.[26−28] It has been demonstrated that the combination of the above two types of polarization groups can produce compounds with excellent SHG properties.[29−31] Guided by this idea and the rule of constructing fluoride carbonate proposed in our previous study,[18] we synthesized a new fluoride carbonate $CsPbCO_3F$, which has Pb^{2+} cations with lone-pair electrons and a suitable ratio of radius between metal ions (Cs/Pb = 1.34). Although the electron lone-pair on the Pb^{2+} almost maintains its spherical shape due to the highly crystal symmetry, it shows higher

Received: August 30, 2013
Published: November 21, 2013

electronic deformation ability than the similar structure compound $KSrCO_3F$. The cooperation of Pb^{2+} $6p$ and $[CO_3]^{2-}$ π^* orbital in the excited state further enhances the nonlinear optical response of $CsPbCO_3F$. For the first time, it is found that the p−π interaction between Pb^{2+} and $[CO_3]^{2-}$ groups within the $[Pb(CO_3)]$ layers is responsible for the remarkable SHG response.

EXPERIMENTAL SECTION

Materials. All of the chemicals were of analytical grade from commercial sources and used without further purification. CsF, $PbCO_3$, Cs_2CO_3, PbF_2, CH_3OH, and C_2H_5OH were purchased from the Shanghai Reagent Factory.

Synthesis. First, polycrystalline $CsPbCO_3F$ was synthesized by solid state reactions. A mixture of CsF (1.52 g, 0.01 mol) and $PbCO_3$ (2.67 g, 0.01 mol) in a molar ratio of 1: 1 was thoroughly ground and loaded into platinum crucibles. It was then heated to 200 °C in flowing CO_2 gas, held for 2 days, and then cooled to room temperature. Second, a mixture of polycrystalline $CsPbCO_3F$ (0.42 g, 1 mmol), PbF_2 (0.098 g, 0.4 mmol), Cs_2CO_3 (0.130 g, 0.4 mmol), and CH_3OH(5.0 mL) was sealed in an autoclave equipped with a Teflon liner (23 mL) and heated at 180 °C for 5 days, followed by slow cooling to room temperature at a rate of 3 °C/h. The product was washed with ethanol, and then dried in air. Colorless, transparent crystals shown in Figure S1 in the Supporting Information were obtained for structure determination.

Single Crystal X-ray Diffraction. Single crystal X-ray diffraction data were collected at room temperature on a Rigaku Mercury CCD diffractometer with graphite-monochromatic Mo Kα radiation (λ = 0.71073 Å). A transparent block of crystal was mounted on a glass fiber with epoxy for structure determination. A hemisphere of data was collected using a narrow-frame method with the ω-scan mode. The data were integrated using the CrystalClear program, and the intensities were corrected for Lorentz polarization, air absorption, and absorption attributable to the variation in the path length through the detector faceplate. Absorption corrections based on the Multiscan technique were also applied. The structure was solved by the direct methods and refined by full-matrix least-squares fitting on F^2 using SHELX-97.[32] All of the structures were verified using the ADDSYM algorithm from the program PLATON,[33] and no higher symmetries were found. Relevant crystallographic data and details of the experimental conditions for $CsPbCO_3F$ are summarized in Table 1. Atomic coordinates and isotropic displacement coefficients are listed in Supporting Information, Table S1. Atomic displacement parameters are listed in Supporting Information, Table S2. Selected bond lengths and angles for $CsPbCO_3F$ are listed in Supporting Information, Table S3.

Powder X-ray Diffraction. X-ray diffraction patterns of polycrystalline materials were obtained on a Rigaku Dmax2500 powder X-ray diffractometer by using Cu Kα radiation (λ = 1.540598 Å) at room temperature in the angular range of 2θ = 5−65° with a scan step width of 0.05° and a fixed time of 0.2 s. The PXRD patterns for $CsPbCO_3F$ showed good agreement with the calculated XRD patterns from the single-crystal models (see Figure S2 in the Supporting Information).

Energy-Dispersive X-ray Spectroscopy (EDS) Analysis. Microprobe elemental analyses were performed on a field emission scanning electron microscope (FESEM, JSM6700F) equipped with an energy dispersive X-ray spectroscope (EDS, Oxford INCA). The collected crystal of $CsPbCO_3F$ was mounted on one flat face and coated with 25 nm carbon. Standards used were $CsAlSi_3O_8$ for cesium, $PbCO_3$ for lead, CaF_2 for fluorine, and graphite for carbon. Three analyses on this sample, one on each of the three visible faces, were performed with a focused beam of 15 keV accelerating voltage and 12 μA emission current.

TG Analysis. The TG scans were measured on a NETZSCH STA 449C simultaneous analyzer. Reference (Al_2O_3) and crystal samples (5−15 mg) were enclosed in Al_2O_3 crucibles and heated from room temperature to 700 °C at a rate of 10 °C/min under a constant flow of nitrogen gas. The TG residues were visually inspected and then analyzed by X-ray powder diffraction after the experiments.

Table 1. Crystal Data and Structure Refinement for $CsPbCO_3F$

formula	$CsPbCO_3F$
formula mass (amu)	419.11
crystal system	hexagonal
space group	$P\bar{6}m2$
a (Å)	5.3888 (8)
c (Å)	5.1071 (14)
α (deg)	90
γ (deg)	120
V (Å^3)	128.44 (4)
Z	1
ρ(calcd) (g/cm^3)	5.419
temp (K)	293(2)
λ(Å)	0.71073
F(000)	176
μ (mm^{-1})	39.74
θ (deg)	3.99−27.19
index range	$-6 \le h \le 6$
	$-6 \le k \le 6$
	$-6 \le l \le 6$
R_1/wR_2 ($I > 2\sigma(I)$)[a]	0.0270/0.0547
R_1/wR_2 (all data)	0.0270/0.0547
GOF on F^2	1.057
absolute structure parameter	0.01 (2)

[a] $R_1(F) = \Sigma||F_o| - |F_c||/\Sigma|F_o|$. $wR_2(F_o^2) = [\Sigma w(F_o^2 - F_c^2)^2/\Sigma w(F_o^2)^2]^{1/2}$

Infrared Spectroscopy. IR spectra were recorded on a Magna 750 Fourier transform infrared (FT-IR) spectrometer as KBr pellets in the range of 4000−400 cm^{-1}.

UV−vis Diffuse Reflectance Spectroscopy. The UV−vis diffuse reflection data were recorded at room temperature using a powder sample with $BaSO_4$ as the standard of 100% reflectance on a PerkinElmer Lamda-900 UV/vis/NIR spectrophotometer and scanned at 200−2500 nm. Reflectance spectra were converted to absorbance using the Kubelka−Munk function.[34,35]

Second-Harmonic Generation. Powder second-harmonic generation (SHG) signals were measured using the experimental method adapted from that reported by Kurtz and Perry[36] with the wavelength of the fundamental (1064 nm doubled to 532 nm). Since SHG efficiencies were known to be strongly dependent on particle size, polycrystalline samples were ground and sieved into the following particle size ranges: 20−44, 44−74, 74−105, 105−149, and 149−210 μm. To make relevant comparisons with known SHG materials, crystalline KDP and $KSrCO_3F$ were also ground and sieved into the same particle size ranges. The samples were pressed between glass microscope cover slides and secured with tape in 1-mm thick aluminum holders containing an 8-mm diameter hole. They were subsequently placed in a light-tight box and irradiated with a pulsed infrared beam (10 ns, 3 mJ, 10 Hz) from a Q-switched Nd:YAG laser at a wavelength of 1064 nm. A cutoff filter was used to limit background flash-lamp light on the sample, and an interference filter (530 ± 10 nm) was used to select the second harmonic for detection with a photomultiplier tube attached to a RIGOL DS1052E 50-MHz oscilloscope. This procedure was then repeated using the standard nonlinear optical materials KDP and $KSrCO_3F$, and the ratio of the second-harmonic intensity outputs was calculated. No index-matching fluid was used in any of the experiments.

Computational Descriptions. The DFT calculations for the experimental crystal structures were performed using the CASTEP code.[37] The generalized gradient approximation (GGA) of Perdew−Burke−Ernzerhof (PBE) form was adopted.[38] The cutoff energy for the plane wave basis was set to be 850 eV. The converge criteria of

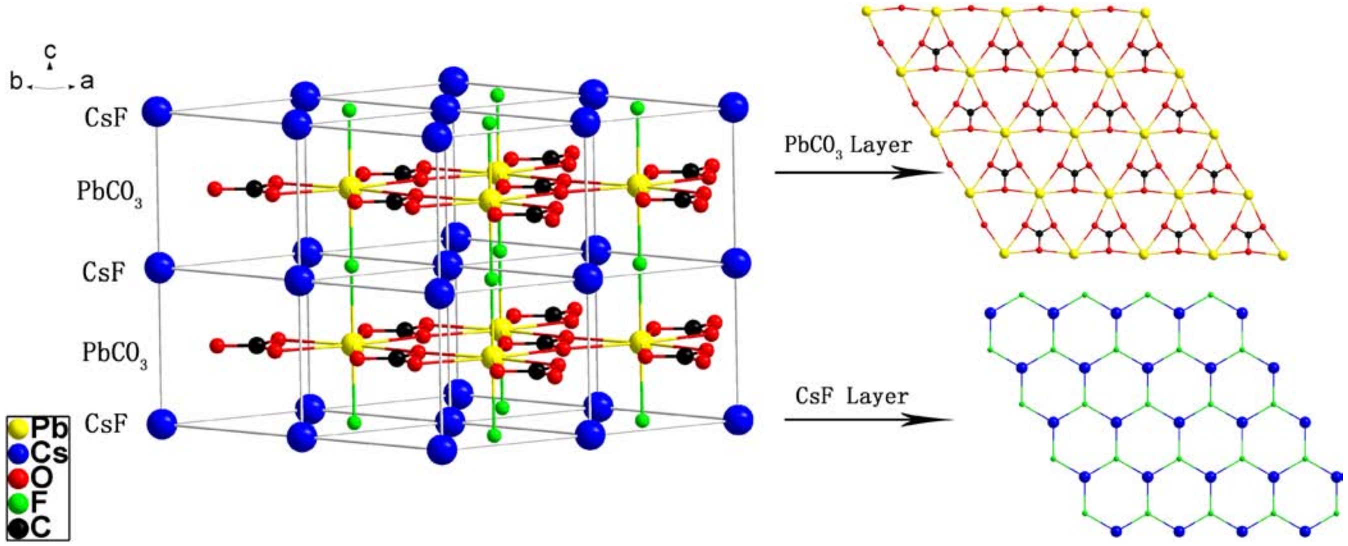

Figure 1. Crystal structure of $CsPbCO_3F$.

energy was 10^{-5} ev/atom. The *k*-points sampling in the Brillioun zone were set to be 3 × 3 × 4 according to the Monkhorst−Pack scheme.[39] The valences of composed atoms were as follow: C $2s^22p^2$, O $2s^22p^4$, F $2s^22p^5$, Cs $5s^25p^66s^1$, Pb $5s^25p^65d^{10}6s^26p^2$, K $3s^23p^64s^1$, Sr $4s^24p^65s^2$. The calculated second-order susceptibilities are expressed in terms of the first-order susceptibilities as follows:

$$\chi^{(2)}_{ijk}(-\omega_3;\, \omega_1,\, \omega_2) = F^{(2)}\chi^{(1)}_{ii}(\omega_3)\chi^{(1)}_{jj}\chi^{(1)}_{kk}(\omega_2) \tag{1}$$

This was derived from a classical anharmonic oscillator (AHO) model[40] where $F^{(2)}$ is the local field correction and is define as

$$F^{(2)} = \frac{m\varepsilon_0^2\varpi_0^2}{N^2e^3d} \tag{2}$$

Here m is the eletron mass, e is the electron charge, ε_0 is the permittivity of free space, N is the atomic density, d is the lattice constant, and ϖ_0 is the atomic resonance frequency. The F values were estimated to be 2.3×10^{-6} esu for $CsPbCO_3F$ and 1.8×10^{-6} esu for $KSrCO_3F$.

The first-order susceptibility $\chi^{(1)}_{ii}$ in the low frequency region is given by $\chi^{(1)}(\omega)_{\mathrm{ii}} = [\varepsilon(\omega)_{\mathrm{ii}} - 1]/(4\pi)$ where the dielectric function is define as

$$\varepsilon_2^{ij}(\omega) = \frac{2e^2\pi}{V_{\mathrm{eff}}\varepsilon_0}\sum_{k,c,v} f_{cv}\frac{p^i_{cv}(k)P^j_{vc}(k)}{E^2_{vc}}\delta[E_{cv}(k) - \hbar\omega] \tag{3}$$

In this expression, $\delta[E_{cv}(k) - \hbar\omega]$ denotes the energy difference between the conduction and valence bands at the k point with absorption of a quantum $\hbar\omega$. f_{cv} represents the difference of Fermi distribution functions of the conduction and valence bands. Because of the well-known underestimation of the band gap for the DFT method, the scissors operation was applied to $E_{cv}(k)$ in the dielectric function calculation, but no further quasiparticle effect is taken into account. The molecular orbital calculation is obtained by using the Guassian 03 software at the B3LYP/lanl2dz level.

■ RESULTS AND DISCUSSION

Crystal Structure. $CsPbCO_3F$ crystallizes into a hexagonal crystal system with an acentric space group of $P\bar{6}m2$ (No. 187). As shown in Figure 1, the structure is made up of alternately stacked layers of $[Pb(CO_3)]_\infty$ and $[CsF]_\infty$. All the adjacent layers are connected by infinite Pb−F−Pb chains parallel to the *c*-axis, forming a three-dimensional network similar to that of $KSrCO_3F$. In the structure, the C atom is coordinated to three O atoms to form a planar CO_3 triangle with C−O bond lengths at 1.282(6) Å and O−C−O bond angles at 120.000(2)°. The lead atom is surrounded by six oxygen atoms and two fluorine atoms, forming a highly symmetrical PbO_6F_2 polyhedron which also exists in $K_{2.70}Pb_{5.15}(CO_3)_5F_3$.[41] The PbO_6F_2 hexagonal bipyramid shares its six equatorial oxygen atoms with three CO_3 groups (Figure 2) to form a flat $PbCO_3$ layer and connects adjacent layers with its apical F atoms along the *c* direction. Within a single $PbCO_3$ layer, the cooperative connection of hexagonal PbO_6 and triangular CO_3 makes all CO_3 groups parallel aligned in the *a*−*b* plane and oriented in the same direction, giving the maximum contribution to a large macroscopic SHG effect. The structure of CsF layers is analogous to that of graphene layers.

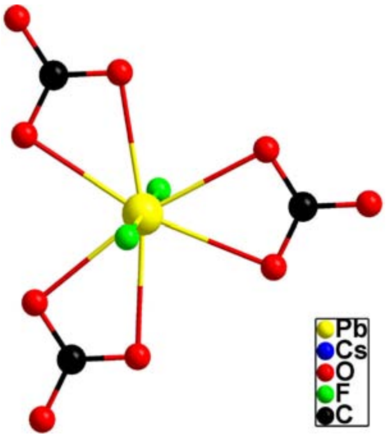

Figure 2. Alignment of CO_3 groups with PbO6F2 polyhedron.

The bond valence sums for $CsPbCO_3F$ are calculated using the formula

$$V_i = \sum_j S_{ij} = \sum_j \exp\{(r_0 - r_{ij})\}/B\} \tag{4}$$

where S_{ij} is the bond valence associated with bond length r_{ij} and r_0 and B (usually 0.37) are empirically determined parameters[42,43] The calculated total bond valence (Cs, 1.221; Pb, 1.686; C, 4.017) indicate that the Cs, Pb, and C atoms are in the oxidation states of +1, +2, and +4, respectively (Supporting Information, Table S4).

Energy-Dispersive X-ray Spectroscopy (EDS) Analysis. The semiquantitative EDS measurements were taken three times from the same $CsPbCO_3F$ crystal that was used for X-ray diffraction analysis. The average Pb/Cs/F molar ratio was 1:1.05:1.17, which is in excellent agreement with that determined from single-crystal XRD analysis. (Supporting Information, Figure S3)

TG Analysis. The thermogravimetric analysis (TGA) curve (Supporting Information, Figure S4) shows that the weight loss of $CsPbCO_3F$ is in one step. $CsPbCO_3F$ is stable up to 280 °C but then continually loses weight up to 460 °C. The weight loss corresponds to the decomposition of the compound through thermal disproportionation, which releases 1 molecule of CO_2. The total weight loss of 10.57% at 460 °C is close to the calculated value of 10.50%. Powder XRD data of the residuals revealed PbO (Supporting Information, Figure S5). So the decomposition reaction is

$$CsPbCO_3F \rightarrow CsF + PbO + CO_2(g)$$

Infrared (IR) Spectroscopy. The IR spectra of $CsPbCO_3F$ revealed C−O vibrations between 1500−650 cm^{-1}. The strong broad bands observed at 1407 cm^{-1} can be assigned to the stretching C−O vibrations. The out-of-plane vibration, δ(OCO), is observed at 843 cm^{-1} as a medium band, and the bending vibration, δ(OCO), should appear at 720−680 cm^{-1} as a medium weak band.[44−47] A strong band, however, was observed in the range of 720−680 cm^{-1} which can be attributed to the overlap between the bending vibration, δ(OCO), and the stretching vibration, ν(Pb−O).[46,47] The ν(Pb−F) vibration can be observed at 407 cm^{-1}.[47] The infrared spectra are presented in Figure S6 of the Supporting Information section.

UV−vis Diffuse Reflectance Spectroscopy. UV−vis diffuse reflectance spectra were collected for $CsPbCO_3F$ (Figure 3). Absorption (K/S) data were calculated from the following Kubelka−Munk function: $F(R) = (1 - R)^2/(2R) = K/S$, where R is the reflectance, K is the absorption, and S is the scattering. In the (K/S)-versus-E plots, extrapolating the linear part of the rising curve to zero provides the onset of absorption. Its UV absorption spectrum exhibits no absorption from 0.30 to 2.5 μm, suggesting that it has wide transparent regions ranging from near-UV to middle-IR. The optical diffuse reflectance spectrum indicates an optical band gap of 4.15 eV, suggesting that $CsPbCO_3F$ is a wide-band gap semiconductor.

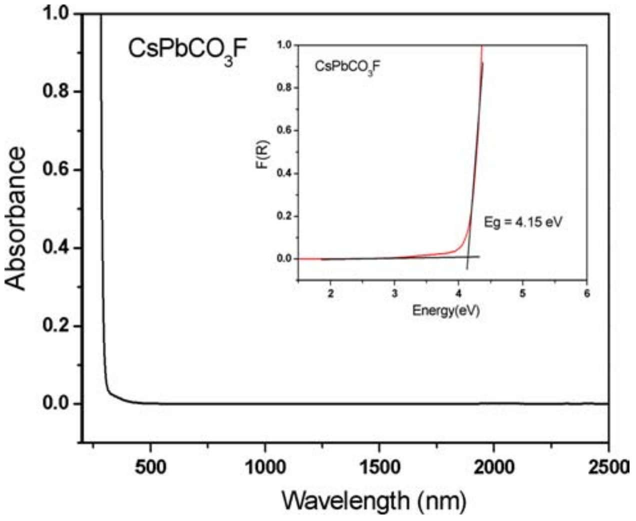

Figure 3. UV absorption spectra and optical diffuse reflectance spectra of $CsPbCO_3F$.

NLO Properties. The curves of SHG signal as a function of particle size from the measurements made on ground crystals for $CsPbCO_3F$ are shown in Figure 4. The results are consistent with phase-matching behaviors according to the rule proposed by Kurtz and Perry[36] (Figure 4b). KDP and $KSrCO_3F$ were used as the reference. $CsPbCO_3F$ exhibited very large SHG responses, ∼13.4 times that of KDP and ∼4 times that of $KSrCO_3F$ (×3.3 KDP)[18] (Figure 4a). Since the reported d_{36} coefficient for KDP is 0.39 pm/V,[48] the derived d_{eff} coefficients for $CsPbCO_3F$ is 5.23 pm/V. The intensity is the largest reported to date among carbonate compounds.

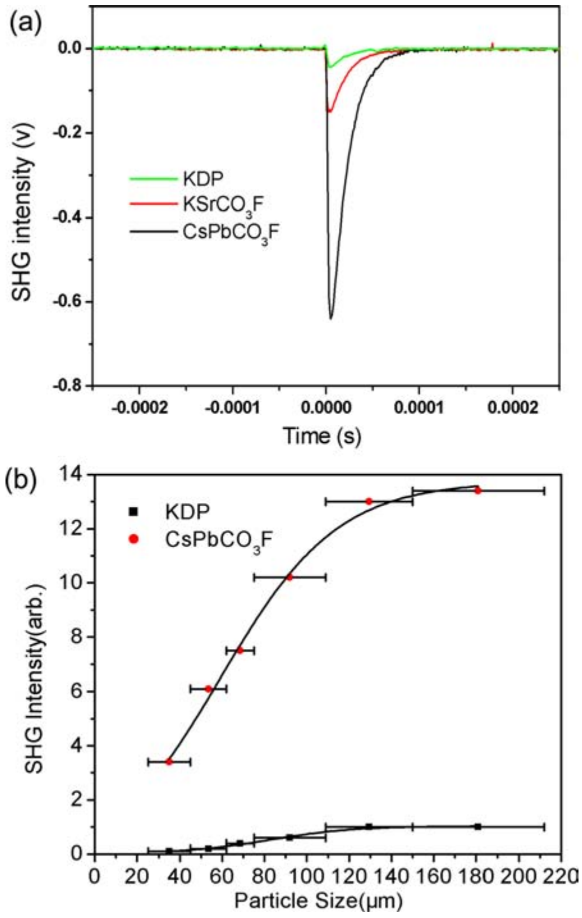

Figure 4. (a) Oscilloscope traces showing SHG intensities for $CsPbCO_3F$ and for KDP and $KSrCO_3F$ as references. (b) phase-matching curve for $CsPbCO_3F$. The solid curve is a guide for the eyes, not a fit to the data.

Theoretical Studies. To gain further insights into the band structure and optical properties of $CsPbCO_3F$, theoretical calculations based on density functional theory (DFT) were performed by using the total-energy CASTEP code.[37−40] The results of band structure calculations (Supporting Information, Figure S7) indicate that $CsPbCO_3F$ is an indirect band semiconductor with a band gap of 3.35 eV, a smaller value than the experimental value as a result of the limitations of DFT methods. The bands just above the Fermi level are predominately derived from Pb-6p, C-2p and some O-2p states. However, the band just below the Fermi level is mostly composed of O-2p, Pb-6p and F-2p states (Figure 5). Unlike the isostructure compound $KSrCO_3F$, in which the charge transfers across the band gap edge are mainly contributed by the O-2p states to the C-2p and O-2p states (Supporting Information, Figure S8), it is found that the charge transfers across the band gap edge are mainly contributed by the O-2p and Pb-6s states to the C-2p, O-2p, and Pb-6p states in $CsPbCO_3F$. Since the space group of $CsPbCO_3F$ belongs to class $\bar{6}m2$, under the restriction of Kleinman's symmetry, only one set of independent SHG tensor components (d_{22}) remains. The calculated frequency-dependent SHG tensor components of $CsPbCO_3F$ are plotted in Supporting Information, Figure S9. The value of d_{22} at the wavelength of 1064 nm (1.165 eV) for $CsPbCO_3F$ is 5.25 pm/V. This value is close to our experimental value, which is 13.4 times that of KDP (d_{36} = 0.39 pm/V).[48]

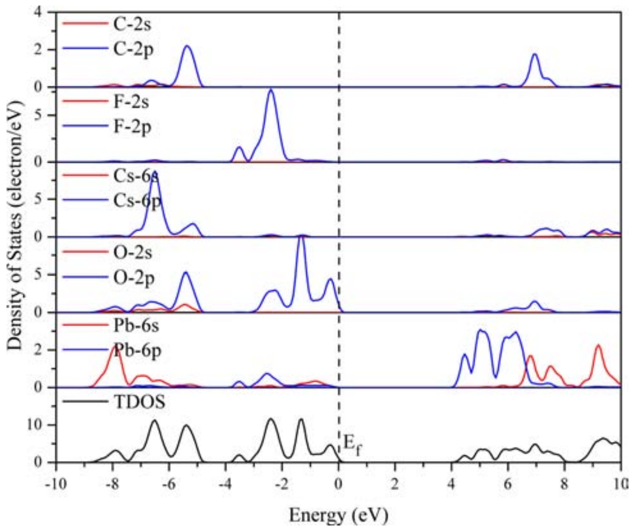

Figure 5. Total and partial density of states of $CsPbCO_3F$. The scissor operator with value 0.8 eV was applied to $CsPbCO_3F$.

NLO Properties and Crystal Structure Relationship. The structure of $CsPbCO_3F$ is noncentrosymmetric but not polar. It is known that, in the polar materials,[49−51] the direction and magnitude of the dipole moments of the polar structural units determine the magnitude of SHG effects such as second-order Jahn−Teller (SOJT) polar displacements of d^0 metal centers, stereochemically lone-pair-active anions (LPAAs), etc. However, in the nopolar materials,[52,53] it is known that the NLO response of a crystal to an external optical electric field is closely related to the induced dipole oscillations in the lattice.[54] This means that the compliance of the dipole moment, rather than the intrinsic dipole moment itself, determines the magnitude of SHG effects. Since the compliance of the dipole moment results from the flexibility of the electronic motion in a chemical bond subjected to the perturbation of the external optical electric field, the more "flexible" the chemical bonds in the microscopic groups are, the larger SHG effect in a crystal will be, provided the resulting second-order susceptibility can be additively superposed. On the basis of the anionic group theory, the contribution to the main SHG coefficients of $CsPbCO_3F$ from the anionic group $[CO_3]$ is dominant. In the structure of $CsPbCO_3F$, the cooperative connection of hexagonal PbO_6 and triangular CO_3 makes all CO_3 groups parallel aligned in the same direction, giving a 100% optimum to maximize contribution to a large macroscopic SHG effect.[55] However in comparison with its isostructural compound $KSrCO_3F$, the sharp SHG increase for $CsPbCO_3F$ may have come from the lone-pair effect on Pb^{2+} cations as expected. However, the ELF calculations (Figure 6) show that $6s^2$ lone-pair on the Pb^{2+} maintains its almost spherical shape except that it is slightly squashed in the z direction, which indicates that the Pb^{2+} cation has an inert or nonstereoactive lone-pair. From the perspective of stereochemistry, the high symmetrical 8-fold coordination environment of Pb^{2+} (Figure 2) limits the distortion of its lone-pair as observed in $K_{2.70}Pb_{5.15}(CO_3)_5F_3$ by P. Shiv Halasyamani.[41] Therefore, $CsPbCO_3F$ would have smaller SHG effects without the enhancement from the lone-pair effect. On the other hand, in comparison to other lead borates or carbonates with a planar triangle structure and similar optical band gaps,[41,56,57] $CsPbCO_3F$ exhibits a significantly larger (over four times larger) SHG response. To determine the origin of the enhanced SHG response, we studied the electronic structure of $CsPbCO_3F$ and $KSrCO_3F$. We composed hypothetic planar $PbCO_3$ and $SrCO_3$ molecules to estimate the valence and conduction band image of the MCO_3 (M = Pb, Sr) layers. As

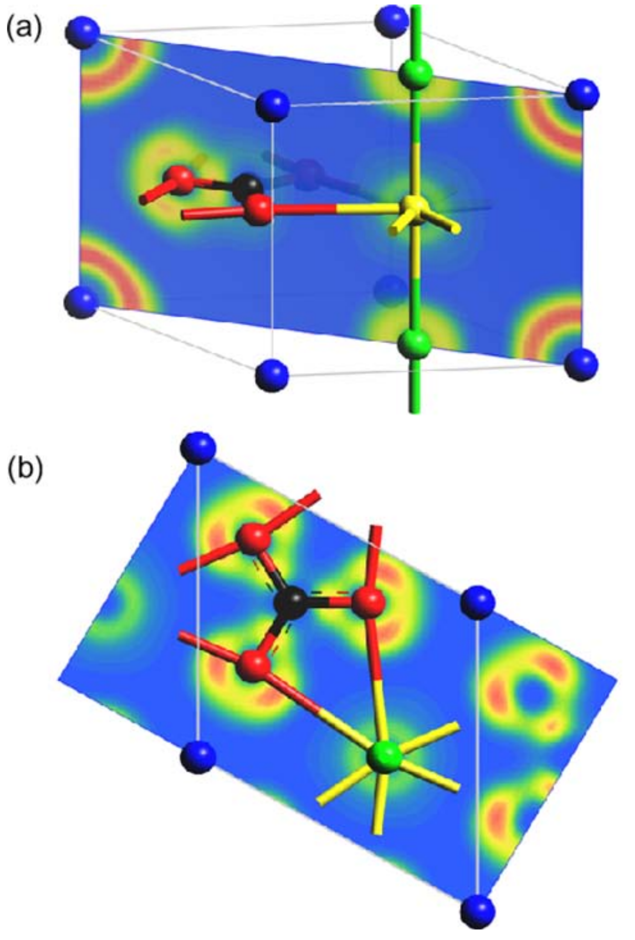

Figure 6. ELF diagram for $CsPbCO_3F$: (a) slice along (110) direction and cutting through Pb and F atoms, (b) slice along (001) direction and cutting through $PbCO_3$ plane. Iso-value increases from blue to red, and the maximum ELF value is scaled to 1. Red spheres represent O atoms, and black, green, and yellow spheres represent C, F, and Pb atoms, respectively.

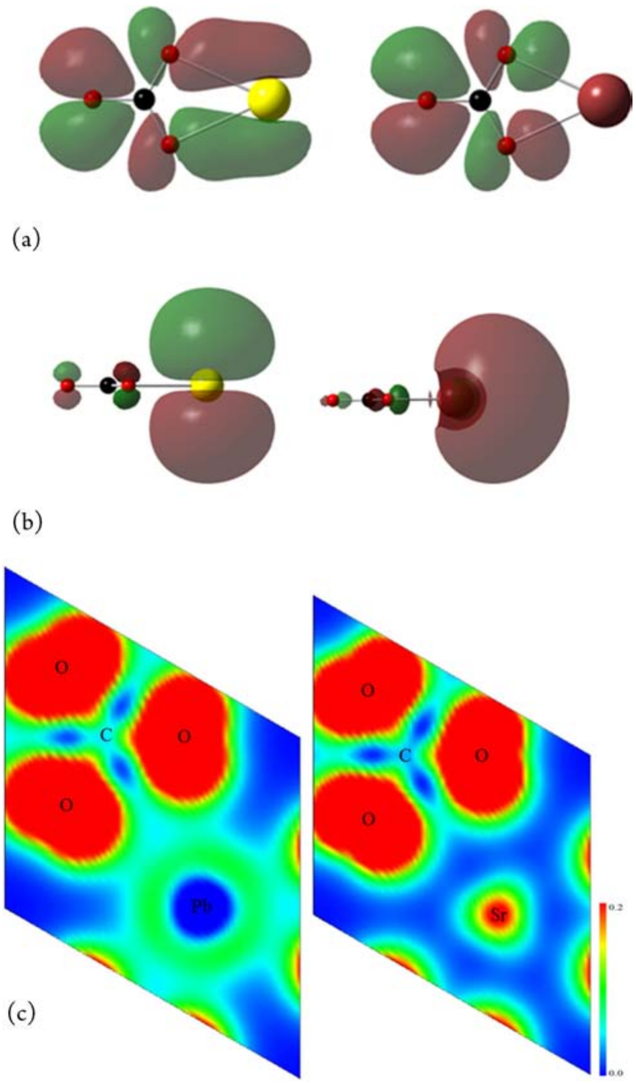

Figure 7. Diagram of the frontier molecular orbitals (iso-value 0.02 au/Å^3): (a) HOMO (top view for molecule $PbCO_3$ (left) and $SrCO_3$ (right), (b) LUMO (side view) for molecule $PbCO_3$ (left) and $SrCO_3$ (right), and (c) partial charge density maps for compound $CsPbCO_3F$ and $KSrCO_3F$ from −4 eV to the Fermi level. The electron density is represented from blue (0.0 e/Å^3) to red (0.2 e/Å^3).

shown in Figure 7a, the highest occupied molecular orbital (HOMO) of a $PbCO_3$ molecule is composed by the $[CO_3]^{2-}$ π orbital and the Pb p_y orbital which shows the delocalized properties over the whole $PbCO_3$ group. For $SrCO_3$, its HOMO is localized in $[CO_3]^{2-}$ π orbital with more ionic bond character. This has also been confirmed by the partial charge density of state representations[58,59] for $CsPbCO_3F$ and $KSrCO_3F$ (Figure 7c) who show that the electron density between Pb−O is about 0.2 au, while there is negligible electron density between Sr and O. The lowest unoccupied molecular orbital (LUMO) of $PbCO_3$ is composed by $[CO_3]^{2-}$ π* orbital and the Pb p_z orbital. As a comparison, the LUMO of $SrCO_3$ is the localized unoccupied Sr 5s orbital (Figure 7b). The participation of Pb^{2+} 6p orbital in LUMO naturally breaks $PbCO_3$ plane's inversion symmetry. Both HOMO and LUMO indicate that $PbCO_3$ plane has more delocalization character than the $SrCO_3$ plane. The calculated static isotropic polarizability of $PbCO_3$ (71 au) is significant larger than the $SrCO_3$ (38 au). This means that $PbCO_3$ has more flexible electronic structure. In fact, when an external electronic field of the same magnitude was applied to both molecules, $PbCO_3$ showed larger electron flowing (Supporting Information, Figure S10) from the Pb atom to the CO_3^{2-} group. Thus the better electron delocalization of $CsPbCO_3F$ possesses larger polarizability. Furthermore, the crystal orbital overlap population analysis (Supporting Information, Figure S11) shows that there are bonding interactions at 10 to 15 eV energy range for Pb−O of $CsPbCO_3F$, while it is all the antibonding contribution at 0 to 15 eV energy range for Sr−O of $KSrCO_3F$. The bonding contribution of Pb−O at the unoccupied band shows that Pb 6p orbital is more energy favorable than the Sr−O in the excitation process. Since more narrow energy gap of $CsPbCO_3F$ corresponds to stronger interaction between the valence and conduction band, it is therefore confirmed that the extremely large SHG efficiency originates from enhancement via p−π interaction between Pb^{2+} and $[CO_3]^{2-}$ within the $[Pb(CO_3)]$ layers, which provides extra flexibility of the electronic motion in the delocalized bond. In $K_{2.70}Pb_{5.15}(CO_3)_5F_3$, the volume density of Pb^{2+} involved in the p−π interaction is about one tenth of that in $CsPbCO_3F$, resulting in a 10 times smaller SHG coefficient than that of $CsPbCO_3F$.

■ CONCLUSION

In summary, a new phase-matchable compound $CsPbCO_3F$ with the largest powder SHG coefficient among carbonates has been synthesized and characterized. Theoretical analyses reveal that the p−π interaction between Pb^{2+} and $[CO_3]^{2-}$ groups within the $[Pb(CO_3)]$ layers are responsible for the remarkable SHG response. The growth of large crystals for further physical property studies is ongoing.

■ ASSOCIATED CONTENT

Ⓢ Supporting Information

The cif data and additional tables and figures as described in the text. This material is available free of charge via the Internet at http://pubs.acs.org.

■ AUTHOR INFORMATION

Corresponding Author

nye@fjirsm.ac.cn

Notes

The authors declare no competing financial interest.

■ ACKNOWLEDGMENTS

This research was supported by the National Natural Science Foundation of China (Nos. 91222204 and 90922035), Main Direction Program of Knowledge Innovation of Chinese Academy of Sciences (Grant No. KJCX2-EW-H03-03) and Special Project of National Major Scientific Equipment Development of China (No. 2012YQ120060).

■ REFERENCES

(1) Luce, J. L. S. K. I.; Keszler, D. A. *Inorg. Chem.* **1994**, *33*, 2453.

(2) Huang, H.; Yao, J.; Lin, Z.; Wang, X.; He, R.; Yao, W.; Zhai, N.; Chen, C. *Angew. Chem., Int. Ed.* **2011**, *50*, 9141.

(3) Wang, S. C.; Ye, N.; Li, W.; Zhao, D. *J. Am. Chem. Soc.* **2010**, *132*, 8779.

(4) Wu, H.; Pan, S.; Poeppelmeier, K. R.; Rondinelli, J. M. *J. Am. Chem. Soc.* **2013**, *135*, 4215.

(5) McMillen, C. D.; Stritzinger, J. T.; Kolis, J. W. *Inorg. Chem.* **2012**, *51*, 3953.
(6) Chen, C.; Liu, G. Z. *Annu. Rev. Mater. Res.* **1986**, *16*, 203.
(7) Chen, C. *Sci. Sin. (Engl. Ed.)* **1979**, *22*, 756.
(8) Chen, C. T.; Wu, B. C.; Jiang, A. D.; You, G. M. *Sci. Sin. B* **1985**, *28*, 235.
(9) Lin, J.; Lee, M. *Phys. Rev. B* **1999**, *60*, 13380.
(10) Chen, C. T.; Wu, Y. C.; Jiang, A. D.; Wu, B. C.; You, G. M.; Li, R. K.; Lin, S. J. *J. Opt. Soc. Am. B* **1989**, *6*, 616.
(11) Lin, Z.; Lin, J.; Wang, Z.; Chen, C. T.; Lee, M. H. *Phys. Rev. B* **2000**, *62*, 1757−1764.
(12) Mei, L.; Wang, Y.; Chen, C.; Wu, B. *J. Appl. Phys.* **1993**, *74*, 7014.
(13) Chen, C. T.; Wang, Y. B.; Wu, B. C.; Wu, K. C.; Zeng, W. L.; Yu, L. H. *Nature* **1995**, *373*, 322.
(14) Pan, F.; Shen, G.; Wang, R.; Wang, X.; Shen, D. *J. Cryst. Growth* **2002**, *241*, 108.
(15) Chen, C. T.; Ye, N.; Lin, J.; Jiang, J.; Zeng, W. R.; Wu, B. C. *Adv. Mater.* **1999**, *11*, 1071.
(16) Chen, C. T.; Lin, Z.; Wang, Z. *Appl. Phys. B: Laser Opt.* **2005**, *80*, 1.
(17) Grice, J. D.; Maisonneuve, V.; Leblanc, M. *Chem. Rev.* **2007**, *107*, 114.
(18) Zou, G. H.; Ye, N.; Huang, L.; Lin, X. S. *J. Am. Chem. Soc.* **2011**, *133*, 20001.
(19) Halasyamani, P. S.; Poeppelmeier, K. R. *Chem. Mater.* **1998**, *10*, 2753.
(20) Maggard, P. A.; Stern, C. L.; Poeppelmeier, K. R. *J. Am. Chem. Soc.* **2001**, *123*, 7742.
(21) Donakowski, M. D.; Gautier, R.; Yeon, J.; Moore, D. T.; Nino, J. C.; Halasyamani, P. S.; Poeppelmeier, K. R. *J. Am. Chem. Soc.* **2012**, *134*, 7679.
(22) Inaguma, Y.; Yoshida, M.; Katsumata, T. *J. Am. Chem. Soc.* **2008**, *130*, 6704.
(23) Zou, G. H.; Ma, Z. J.; Wu, K. C.; Ye, N. *J. Mater. Chem.* **2012**, *22*, 19911.
(24) Sun, C. F.; Hu, C. L.; Xu, X.; Yang, B. P.; Mao, J. G. *J. Am. Chem. Soc.* **2011**, *133*, 5561.
(25) Zhang, J.; Zhang, Z.; Zhang, W.; Zheng, Q.; Sun, Y.; Zhang, C.; Tao, X. *Chem. Mater.* **2011**, *23*, 3752.
(26) Wu, H.; Pan, S.; Poeppelmeier, K. R.; Li, H.; Jia, D.; Chen, Z.; Fan, X.; Yang, Y.; Rondinelli, J. M.; Luo, H. *J. Am. Chem. Soc.* **2011**, *133*, 7786.
(27) Becker, P. *Adv. Mater.* **1998**, *10*, 979.
(28) Pan, S.; Smit, J. P.; Watkins, B.; Marvel, M. R.; Stern, C. L.; Poeppelmeier, K. R. *J. Am. Chem. Soc.* **2006**, *128*, 11631.
(29) Kong, F.; Huang, S. P.; Sun, Z. M.; Mao, J. G.; Cheng, W. D. *J. Am. Chem. Soc.* **2006**, *128*, 7750.
(30) Zhang, W. L.; Cheng, W. D.; Zhang, H.; Geng, L.; Lin, C. S.; He, Z. Z. *J. Am. Chem. Soc.* **2010**, *132*, 1508.
(31) Huang, Y. Z.; Wu, L. M.; Wu, X. T.; Li, L. H.; Chen, L.; Zhang, Y. F. *J. Am. Chem. Soc.* **2010**, *132*, 12788.
(32) Sheldrick, G. M. *Acta Crystallogr. Sect. A* **2008**, *64*, 112.
(33) Spek, A. L. *J. Appl. Crystallogr.* **2003**, *36*, 7.
(34) Kubelka, P.; Munk, F. Z. *Tech. Phys.* **1931**, *12*, 593.
(35) Tauc, J. *Mater. Res. Bull.* **1970**, *5*, 721.
(36) Kurtz, S. K.; Perry, T. T. *J. Appl. Phys.* **1968**, *39*, 3798.
(37) Segall, M. D.; Lindan, P. J. D.; Probert, M. J.; Pickard, J.; Hasnip, P. J.; Clark, S. J.; Payne, M. C. *J. Phys.-Condense Matter* **2002**, *14*, 2717.
(38) Perdew, J. P.; Burke, K.; Ernzerhof, M. *Phys. Rev. Lett.* **1996**, *77*, 3865.
(39) Monkhorst, H. J.; Pack, J. D. *Phys. Rev. B.* **1976**, *13*, 5188.
(40) Boyd, R. W. *Nonlinear Optimization*; Academic Press: New York, 1992 .
(41) Tran, T. Thao.; Halasyamani, P. S. *Inorg. Chem.* **2013**, *52*, 2466.
(42) Brown, I. D.; Altermatt. *D. Acta Crystallogr.* **1985**, *B41*, 244.
(43) Brese, N. E.; O'Keeffe, M. *Acta Crystallogr.* **1991**, *B47*, 192.
(44) Donoghue, M.; Hepburn, P. H.; Ross, S. D. *Spectrochim. Acta. A* **1971**, *27*, 1065.
(45) Andersen, F. A.; Brecevic, L. *Acta Chem. Scand.* **1991**, *45*, 1018.
(46) Refat, M. S.; Elsabawy, K. M. *Bull. Mater. Sci.* **2011**, *34*, 873.
(47) Nakamoto, K. *Infrared and Raman Spectra of Inorganic and Coordination Compounds*; John Wiley: Hoboken, N.J., 2007.
(48) Eckardt, R. C.; Masuda, H.; Fan, Y. X.; Byer, R. L. *IEEE J.Quantum Electron.* **1990**, *26*, 922.
(49) Sun, C. F.; Hu, C. L.; Mao, J. G. *Chem. Commun.* **2012**, *48*, 4220.
(50) Goodey, J.; Broussard, J.; Halasyamani, P. S. *Chem. Mater.* **2002**, *14*, 3174.
(51) Porter, Y.; Halasyamani, P. S. *J. Solid State Chem.* **2003**, *174*, 441.
(52) Wang, Y.; Pan, S. L.; Yu, H. W.; Su, X.; Zhang, M.; Zhang, F. F.; Han, J. *Chem. Commun.* **2013**, *49*, 306.
(53) Zhang, J. J.; Zhang, Z. H.; Sun, Y. X.; Zhang, C. Q.; Zhang, S. J.; Tao, X. T. *J. Mater. Chem.* **2012**, *22*, 9921.
(54) Butcher, P. N.; Cotter, D. *The Elements of Nonlinear Optics*; Cambridge University Press: UK, 1990.
(55) Ye, N.; Chen, Q. X; Wu, B. C; Chen, C. T. *J. Appl. Phys.* **1998**, *84*, 1.
(56) Chen, Z. H.; Pan, S. L.; Yang, Z. H.; Dong, X. Y.; Su, X.; Yang, Y. *J. Mater. Sci.* **2013**, *48*, 2590.
(57) Zhao, W. W.; Pan, S. L.; Dong, X. Y.; Chen, Z. H. *Mater. Res. Bull.* **2012**, *47*, 947.
(58) Kresse, G.; Hafner. *J. Phys. Rev. B: Condens. Matter* **1993**, *48*, 13115.
(59) Kresse, G.; Furthmüller, J. *Comput. Mater. Sci.* **1996**, *6*, 15.